

# Remote-Focussing for Volumetric Imaging in a Contactless and Label-Free Neurosurgical Microscope

Jiahe Cui<sup>1,\*</sup>, Raphaël Turcotte<sup>1,2</sup>, Karen Hampson<sup>1</sup>, Nigel J. Emptage<sup>2</sup>,  
and Martin J. Booth<sup>1</sup>

<sup>1</sup>Department of Engineering Science, University of Oxford, Parks Road, Oxford OX1 3PJ, United Kingdom

<sup>2</sup>Department of Pharmacology, University of Oxford, Mansfield Road, Oxford OX1 3QT, United Kingdom

\*jiahe.cui@eng.ox.ac.uk

**Abstract:** We present a compact and contactless reflectance confocal neurosurgical microscope that allows remote-focussing via a deformable mirror for volumetric imaging. Wavefront analysis was performed and remote-focussing was demonstrated in mouse calvaria. © 2021 The Author(s)

## 1. Introduction

Visual guidance at the cellular level during neurosurgical procedures is essential for enabling maximal tumour resection with minimal damage to adjacent brain tissue. However, most conventional surgical microscopes are not optimised for visualisation of individual cells. Modern endoscopic probes provide high spatial resolution, but the need for direct tissue contact makes it susceptible to erythrocyte contamination [1]. Label-free imaging is highly desirable to eliminate complexities from fluorophore uptake and toxicity, injection timings, dose constraints, etc. [2]. Meanwhile, direct perception of depth information is important for understanding complex relationships of neuroanatomical structures in the peripheral environment [3]. There are many ways to achieve volumetric imaging. Remote-focussing (RF) using a dynamic device, such as a deformable mirror (DM), is one of these methods that can permit fast, inertia-free axial refocussing by reshaping of the DM membrane [4].

Here we present our developments upon a compact and contactless reflectance confocal neurosurgical microscopes [5] by integrating a DM and a custom Shack-Hartmann wavefront sensor (SHWS). A lateral resolution of  $<1.2\text{ }\mu\text{m}$  and axial resolution of  $<5.8\text{ }\mu\text{m}$  was maintained from our previous work, as well as an effective working distance of 20 mm. Axial-refocussing via the deformable mirror was achieved for a  $150\text{ }\mu\text{m}$  depth range. Wavefront analysis was performed and RF results were demonstrated in frozen mouse calvaria.

## 2. System setup

A schematic of the main system setup is illustrated in Figure 1(a) with details extensively introduced in [5]. Major modifications include the integration of a DM (DM-69, Alpao) to allow for large range RF. A separate wavefront sensing path was added to position a custom SHWS at a conjugate pupil plane to the DM membrane. A  $150\text{ }\mu\text{m}$  pitch, 5.2 mm focal length microlens array (MLA150-7AR-M, Thorlabs) was attached to a xiQ CMOS camera (MQ042MG-CM, Ximea) to form the SHWS. 14 lenslets were illuminated across the pupil diameter (148 lenslets in total) to sample the DM membrane with approximately 2:1 lenslet-actuator ratio.

## 3. Remote-focussing calibration

Calibration of the DM actuator voltages required for RF at different depths was enabled by a closed-loop sensor-based adaptive optics (AO) scheme. A SHWS was used to directly sense the shape of the wavefront. First, the DM was calibrated to find the relationship between voltage values sent to each DM actuator and the amount of membrane deformation. To achieve this, a positive and negative voltage of the same magnitude were sequentially applied to each actuator, and the corresponding  $x$ - and  $y$ -slope values were obtained for all lenslets of the SHWS to construct the DM influence function matrix. The final DM control matrix was obtained by pseudo-inverse, and was then used throughout the closed-loop AO correction process via an integral controller to convert between SHWS slope values and DM actuator voltages for reshaping of the DM membrane.

Voltages for RF were calibrated by axially displacing a piece of white card an amount  $\Delta d\text{ }\mu\text{m}$  away from the objective focal plane using a sample translation stage for each calibration step, and correcting for the displacement via closed-loop AO correction. Displacements were introduced along both  $+z$ -axis and  $-z$ -axis to enable

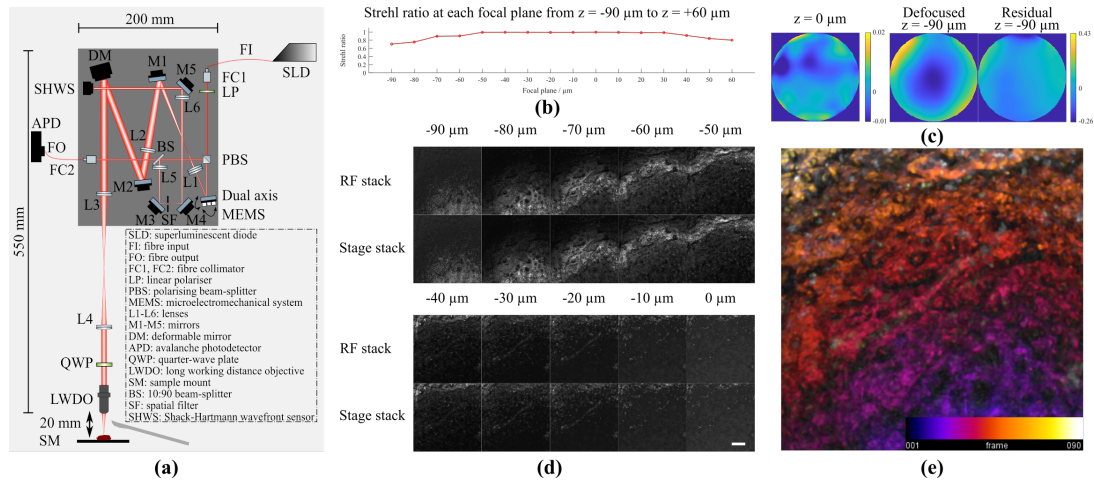


Fig. 1: System setup and remote-focussing results. (a) Schematic of system setup. (b) Strehl ratio for each RF calibration step. (c) Reconstructed wavefronts for natural focus ( $z = 0 \mu\text{m}$ ) and  $z = -90 \mu\text{m}$  before and after closed-loop AO correction. (d) 90- $\mu\text{m}$  deep axial stacks obtained in frozen mouse calvaria. (e) Colour projection for 1  $\mu\text{m}$  interval RF stack images. Scale bar: 100  $\mu\text{m}$ .

refocussing on either side of the natural focal plane. Linear interpolation was subsequently performed to acquire voltages for finer refocussing intervals. All voltages were then routinely loaded upon software initialisation.

#### 4. Results

RF calibration was performed according to the procedure in Section 3, with  $\Delta d$  set to 10  $\mu\text{m}$  and a fine refocussing interval of 0.1  $\mu\text{m}$ . An axial refocussing range of  $-90 \mu\text{m} \sim +60 \mu\text{m}$  was achieved for calculated Strehl ratios of above 0.7. Results for each calibration step are given in Figure 1(b). Further characterisations of the reconstructed wavefront are given in Figure 1(c) for that obtained at the natural focus as well as comparison between defocused and residual wavefronts before and after closed-loop AO correction at  $z = -90 \mu\text{m}$ .

Remote-focussing performance was demonstrated within frozen mouse calvaria. Volumetric stacks were obtained by acquiring images with 10  $\mu\text{m}$  axial steps over a 90  $\mu\text{m}$  depth range from the surface of the calvaria (Figure 1(d)). Comparison was made between scanning sequentially through multiple depths using the pre-calibrated DM actuator voltages (Figure 1(d), top row); and axial translation of the sample stage (Figure 1(d), bottom row). Results validate that refocussing via deformation of the DM membrane was capable of precisely locating the target focal plane throughout the full 90  $\mu\text{m}$  depth range, with no noticeable decrease in spatial resolution or image intensity. To fully appreciate the fine refocussing ability of the DM enabled by linear interpolation of calibrated actuator voltages, a volumetric stack with 1  $\mu\text{m}$  intervals was obtained at the same region. A full colour projection is demonstrated in Figure 1(e) for simultaneous analysis of depth information at each layer.

#### 5. Conclusion

We present a volumetric imaging method in a compact and contactless reflectance confocal neurosurgical microscope by means of remote-focussing via a deformable mirror. Performance was validated by comparison with axial stacks acquired by sample stage translation for a 90  $\mu\text{m}$  depth range in frozen mouse calvaria.

#### References

1. T. Sankar, *et. al.*, “Miniaturized handheld confocal microscopy for neurosurgery: results in an experimental glioblastoma model,” *Neurosurg.* **66**(2), 410–418 (2010).
2. E. Belykh, *et. al.*, “Intraoperative fluorescence imaging for personalized brain tumor resection: Current state and future directions,” *Front. Surg.* **3**, 55 (2016).
3. L. Ma, *et. al.*, “Comprehensive review of surgical microscopes: technology development and medical applications,” *J. Biomed. Opt.* **26**(1), 010901 (2021).
4. Y. Yang, *et. al.*, “Adaptive optics enables aberration-free single-objective remote focusing for two-photon fluorescence microscopy,” *Biomed. Opt. Express* **12**(1), 354–366 (2021).
5. J. Cui, *et. al.*, “Compact and contactless reflectance confocal microscope for neurosurgery,” *Biomed. Opt. Express* **11**(8), 4772–4785 (2020).